Physics of Fluids

Discovery of the zeroth law of helicity spectrum in the pre-inertial range of wall turbulence

Cite as: Phys. Fluids **34**, 071401 (2022); https://doi.org/10.1063/5.0093998
Submitted: 31 March 2022 • Accepted: 10 June 2022 • Published Online: 06 July 2022

Sk Zeeshan Ali and Subhasish Dey

Physics of Fluids PERSPECTIVE scitation.org/journal/phf

Discovery of the zeroth law of helicity spectrum in the pre-inertial range of wall turbulence

Cite as: Phys. Fluids **34**, 071401 (2022); doi: 10.1063/5.0093998
Submitted: 31 March 2022 · Accepted: 10 June 2022 ·
Published Online: 6 July 2022

Sk Zeeshan Ali[1,a)] and Subhasish Dey[2,3,a)]

AFFILIATIONS

[1]Department of Civil Engineering, Indian Institute of Technology Hyderabad, Telangana 502284, India
[2]Department of Civil Engineering, Indian Institute of Technology Kharagpur, West Bengal 721302, India
[3]Department of Hydraulic Engineering, State Key Laboratory of Hydro-Science and Engineering, Tsinghua University, Beijing 100084, China

[a)]**Authors to whom correspondence should be addressed:** zeeshan@ce.iith.ac.in and sdey@iitkgp.ac.in

ABSTRACT

We report an unprecedented existence of the zeroth law of helicity spectrum (i.e., the helicity spectrum becomes independent of the wavenumber) in the transition from production range to inertial range, herein termed the pre-inertial range, of wall turbulence. The zeroth law is explained by the superposition effect of the forward joint cascade of energy and helicity caused by twisting and stretching of wall-attached superstructures in an equilibrium layer. The phenomenological model perfectly predicts the zeroth law in the pre-inertial range. Experimental data support the existence of the zeroth law.

I. INTRODUCTION

Three-dimensional (3D) incompressible Navier–Stokes turbulence holds two inviscid invariants: energy and helicity (scalar product of fluid velocity and vorticity). The helicity is a measure of knotting and linking of vortex lines.[1] The classical picture of the 3D turbulence is based on the forward energy cascade from energy-carrying large to energy-dissipating small scales. However, in a wide variety of natural flows, where parity-invariance is broken, the presence of non-zero mean helicity yields a forward joint cascade of both energy and helicity from large to small scales.[2] Recent direct numerical simulation (DNS) has shown that the forward joint cascade is compatible because of the presence of scale-dependent phase orientation between velocity and vorticity fluctuations.[3] The forward joint cascade was observed in atmospheric boundary layer measurements,[4] numerical simulations of homogeneous and isotropic turbulence,[5–8] and the DNS of the Ekman boundary layer.[9] At large Reynolds numbers, the forward joint cascade yields three spectral ranges in the helicity spectrum $H(k)$ (where k is the wavenumber)—(i) the production range, where no specific spectral law has been recognized; (ii) the inertial range, where the spectrum obeys $H(k) \sim k^{-5/3}$; and (iii) the dissipation range, which displays the spectral decay due to the dissipation. Another spectral range $H(k) \sim k^{-4/3}$ was argued in the transition from inertial range to dissipation range based on the timescale for helicity transfer at large wavenumbers.[10]

In this Perspective article, we show that in a wall turbulence, the helicity spectrum in the pre-inertial range becomes independent of the wavenumber as $H(k) \sim k^0$, which is called here the zeroth law of helicity spectrum. Although signature of the zeroth law exists in experimentally observed spectra,[4] this law has never been recognized so far. Moreover, its origin in a wall turbulence is still unknown. The purpose of this Perspective article is to report the existence of the zeroth law of helicity spectrum and its origin based on a phenomenological model of wall turbulence.

The cascades of energy and helicity were previously explained by the vortex stretching and twisting, respectively.[11] However, the vortex stretching was also reported to take part in the helicity cascade.[12] Recent DNS data of a wall turbulence have evidenced the dual channels of the helicity cascade, where the dynamics are governed by the vortex twisting and stretching.[13] Herein, the forward joint cascade of energy and helicity in a wall turbulence is explained by the twisting and stretching of wall-attached superstructures within an equilibrium layer (Fig. 1). The superstructures are large elongated structures, having a length scale of approximately 15–20 times the external flow scale L, which is of the order of the boundary layer thickness.[14] In particular, their existence was evidenced in a pipe, a channel, a boundary layer, and atmospheric surface layer flows,[15] and in general, they are considered to be ubiquitous for wall turbulence at large Reynolds numbers.[14]

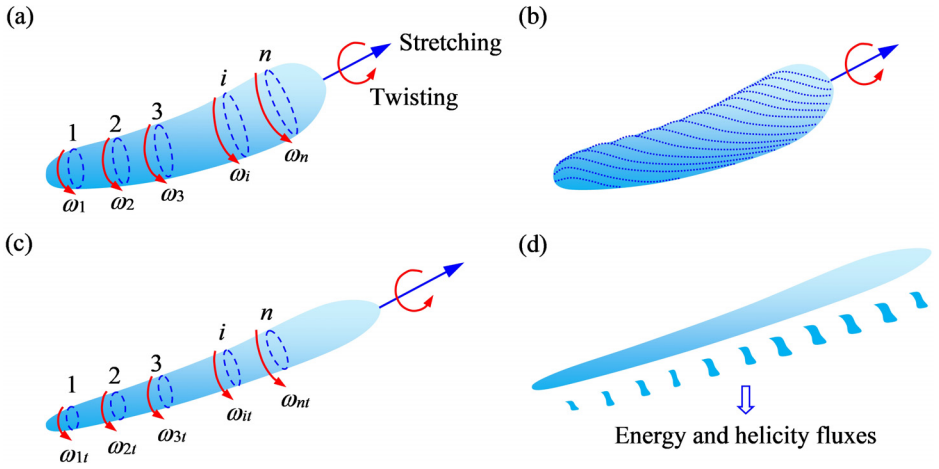

FIG. 1. (a) A superstructure subject to twisting and stretching, (b) formation of small-scale helices, (c) spin-up of the superstructure at later time, and (d) breakdown of the superstructure transmitting the energy and helicity fluxes toward the wall.

II. CONCEPTUAL FRAMEWORK

Let us consider twisting and stretching of a superstructure with different cross sections marked as 1, 2, 3,…, n having vorticities ω_1, ω_2, ω_3, … ω_n ($\omega_1 < \omega_2 < \omega_3 < \cdots < \omega_n$) [see Fig. 1(a)]. The twisting action causes vorticity gradient along the filament, and, subsequently, the superstructure deforms into helices [Fig. 1(b)]. Due to the presence of axial velocity, the helicity generated at a given cross section is transferred toward the small scales. However, because of the stretching, the cross-sectional area reduces to satisfy the mass conservation [Fig. 1(c)]. As a result, the vorticity enhances to conserve the angular momentum ($\omega_1 < \omega_{1t}$, $\omega_2 < \omega_{2t}$,…, $\omega_n < \omega_{nt}$). This spin-up causes energy to cascade toward the small-scales. Therefore, the twisting and stretching of superstructure yield transfer of energy and helicity into small-scales. After a certain time, further twisting and stretching result in a breakdown of the superstructure. As a result, both the energy and helicity fluxes carried by the small-scale helices are transported toward the wall [Fig. 1(d)].

The energy and helicity fluxes are obtained as $\phi_E \sim kE(k)/t_E$ and $\phi_H \sim kH(k)/t_E$, respectively.[2] Here, $E(k)$ is the energy spectrum and $t_E(k) \sim \left(\int_0^k k^2 E(k)\mathrm{d}k\right)^{-1/2}$ is the distortion time governed by the time-scale associated with the energy transfer. Setting the energy and helicity dissipation rates as $\varepsilon = 2\nu \int_0^\infty k^2 E(k)\mathrm{d}k$ and $\eta = 2\nu \int_0^\infty k^2 H(k)\mathrm{d}k$, respectively (where ν is the coefficient of kinematic viscosity), and using the Kolmogorov scaling $E(k) \sim \varepsilon^{2/3}k^{-5/3}$ yield the helicity spectrum in the inertial range as[2,16]

$$H(k) \sim \eta\left[k^5 E(k)\right]^{-1/2} \sim \eta\varepsilon^{-1/3}k^{-5/3}. \tag{1}$$

In the phenomenology of wall-attached superstructures within the equilibrium layer [Fig. 2(a)], each superstructure transfers the energy and helicity fluxes toward the wall. Therefore, the net energy and helicity fluxes at any wall-normal distance can be obtained by superposition of the energy and helicity fluxes transmitted by all superstructures above that level [Fig. 2(b)]. This superposition effect can be inferred from Townsend's hypothesis.[17] As the characteristic length l of the superstructure scales with wall-normal distance ($l \sim z$), the energy and helicity fluxes enhance with wavenumber k ($\sim z^{-1}$). So, at an arbitrary distance z_i, these fluxes increase with k up to $k = z_i^{-1}$ because of the contributions from all superstructures above $z = z_i$. On the other hand, for $k > z_i^{-1}$, the energy and helicity fluxes attain their local dissipation rates ε_l and η_l, respectively. This suggests

$$\phi_E(L^{-1} < k \le z^{-1}) = \phi_{E1} + \phi_{E2} + \phi_{E3} + \cdots + \phi_{Ei}, \tag{2}$$

$$\phi_E(z^{-1} < k < k_d) = \varepsilon_l, \tag{3}$$

$$\phi_H(L^{-1} < k \le z^{-1}) = \phi_{H1} + \phi_{H2} + \phi_{H3} + \cdots + \phi_{Hi}, \tag{4}$$

$$\phi_H(z^{-1} < k < k_d) = \eta_l, \tag{5}$$

where k_d is the dissipation wavenumber. Dimensional argument suggests $\varepsilon \sim u_l^2/t_E$, where u_l is the amplitude of velocity fluctuation associated with scale l. The distortion time t_E is set as $t_E \sim l/u_l$. Within the equilibrium layer, the scaling relationships, such as $l \sim z$ and $u_l \sim u_*$,[17] establish the law of the wall,[18] where u_* is the shear velocity. This makes $t_E \sim z/u_* \sim (u_* k)^{-1}$ (since $k \sim z^{-1}$). Thus, ε reads $\varepsilon \sim u_*^3/z \sim u_*^3 k$. The turbulent helicity within the equilibrium layer can be set as follows:[3] $h \sim u_l\omega_l \sim u_l^2/l$ (since $\omega_l \sim u_l/l$, where ω_l is the amplitude of vorticity fluctuation associated with scale l), yielding $h \sim u_*^2/z \sim u_*^2 k$. Similar scaling was found in the DNS of the Ekman boundary layer via a different route as $h \sim \varepsilon/u_l \sim u_*^2/z$.[9] Therefore, the helicity dissipation rate η ($= h/t_E$) is $\eta \sim u_*^3/z^2 \sim u_*^3 k^2$. With this phenomenological model, for a given wall-normal distance z within the equilibrium layer, Eq. (1) predicts

$$H(L^{-1} < k \le z^{-1}) \sim \eta\varepsilon^{-1/3}k^{-5/3} \sim u_*^3 k^2 (u_*^3 k)^{-1/3} k^{-5/3} \sim u_*^2 k^0, \tag{6}$$

$$H(z^{-1} < k < k_d) \sim \eta_l \varepsilon_l^{-1/3} k^{-5/3}. \tag{7}$$

Equation (6) predicts the zeroth law of helicity spectrum in the pre-inertial range ($L^{-1} < k \le z^{-1}$).

From the above conceptual flow physics, the zeroth law of helicity spectrum in the pre-inertial range of wall turbulence states as follows:

> *At large Reynolds numbers in a wall turbulence, the superposition effect of the forward joint cascade of energy and helicity caused by twisting and stretching of wall-attached superstructures in an equilibrium layer yields a pre-inertial range (i.e., transition from production range to inertial range) with the helicity spectrum to be independent of wavenumber.*

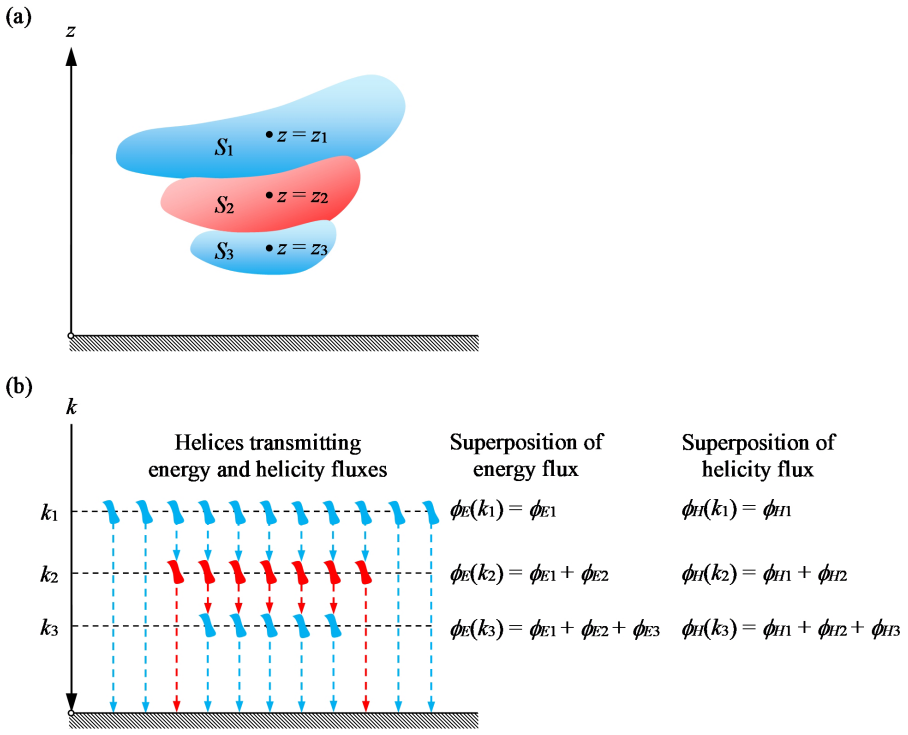

FIG. 2. (a) Superstructures S_1, S_2, and S_3 at distances z_1, z_2, and z_3 ($z_1 > z_2 > z_3$) from the wall and (b) transformation of the physical domain to the wavenumber domain ($k \sim z^{-1}$) with $k_1 < k_2 < k_3$ showing the superposition effect of energy and helicity fluxes at levels z_2 ($\sim k_2^{-1}$) and z_3 ($\sim k_3^{-1}$). For clarity, only three superstructures S_1, S_2, and S_3 are shown.

It is worth mentioning that for $L < k \leq z^{-1}$, the energy spectrum follows $E(k) \sim \varepsilon^{2/3}k^{-5/3} \sim (u_*^3 k)^{2/3}k^{-5/3} \sim u_*^2 k^{-1}$, which shows the "−1" spectral law of energy spectrum in a wall turbulence, as reported previously.[19]

III. EVIDENCE OF THE ZEROTH LAW

Quantification of the spectral characteristics of turbulent helicity through experimental measurements has been challenging and extremely rare. This is because of the difficulties in measuring the velocity and the vorticity components simultaneously. Moreover, a direct estimate of the vorticity from the velocity field is another complicated aspect. However, by measuring the circulation along a given contour, a precise estimation of the area-averaged vorticity can be obtained. By means of a three-component circulation meter and an acoustic anemometer, combined measurements of the circulation and velocity components in the atmospheric boundary layer have been reported in the literature.[4] In September 2004, the measurements were taken at an elevation of 46 m at the Zvenigorod scientific station, Institute of Atmospheric Physics. It was found that the effects of the surface heterogeneity are minimal at an elevation of 46 m. To be specific, the circulation was measured by a quadratic contour having the side lengths of 0.5 m, and the distance of the velocity measuring point from the contour center was 1 m. Further details of the measurements are given in Ref. 4.

The experimental evidence of the zeroth law of helicity spectrum is shown in Fig. 3. Both the experimentally observed helicity and energy spectra corresponding to the atmospheric surface layer at an elevation of $z = 46$ m having a time-averaged wind speed u_m of about 2 m s^{-1} are shown in Fig. 3. The external flow scale L defining the boundary layer thickness was approximately 700 m. The spectra in Fig. 3 were obtained from the time signal. From the time series of the velocity and vorticity for each component, the scalar multiplication results in the time series for the helicity components to which the Fourier frequency analysis was applied. With the frequency f, the frequency spectrum of helicity $H(f)$ was, therefore, converted to the wavenumber spectrum of helicity $H(k)$ by applying the simplest form of Taylor hypothesis, i.e., $k = f/u_m$ and $H(k) = u_m H(f)$. Likewise, the energy spectrum $E(k)$ was obtained. For each spectrum, the total number of data points in Fig. 3 is 107 with finest wavenumber spacings of 3.123×10^{-5} and 2×10^{-3} m^{-1} in the production range and the inertial range, respectively. The theoretical bounds of the pre-inertial range, given by $L^{-1} < k \leq z^{-1}$ (i.e., 1.4×10^{-3} m$^{-1} < k \leq 2.2 \times 10^{-2}$ m^{-1}), are also shown.

The zeroth law of helicity spectrum [$H(k) \sim k^0$] in the pre-inertial range, as predicted in Eq. (6), is shown in Fig. 3. Specifically, the experimental data of $H(k)$ follow a flat spectrum in the range 1.4×10^{-3} m$^{-1} < k < 6 \times 10^{-3}$ m^{-1}. In Fig. 3, the total number of data points in the range 1.4×10^{-3}m$^{-1} < k < 6 \times 10^{-3}$ m^{-1} is 16. However, just above $k = 7 \times 10^{-3}$ m^{-1}, the helicity spectrum falls off slightly, displaying another flat spectrum from $k = 10^{-2}$ m^{-1} to $k = z^{-1}$ (i.e., 2.2×10^{-2} m^{-1}). The discontinuity in the flat spectrum could be due to the operation on the mast positioned at $z = 46$ m (i.e., $k = 2.2 \times 10^{-2}$ m^{-1}), disturbing the zeroth law to some extent toward low wavenumber range, i.e., 7×10^{-3} m$^{-1} < k < 2.2 \times 10^{-2}$ m^{-1}, as a result of either the natural fluctuations of the spectrum or the vortex shedding. The discontinuity may disappear with other boundary condition or longer averaging. This remains a future scope of research. However, as far as the pre-inertial range ($L^{-1} < k \leq z^{-1}$) is concerned,

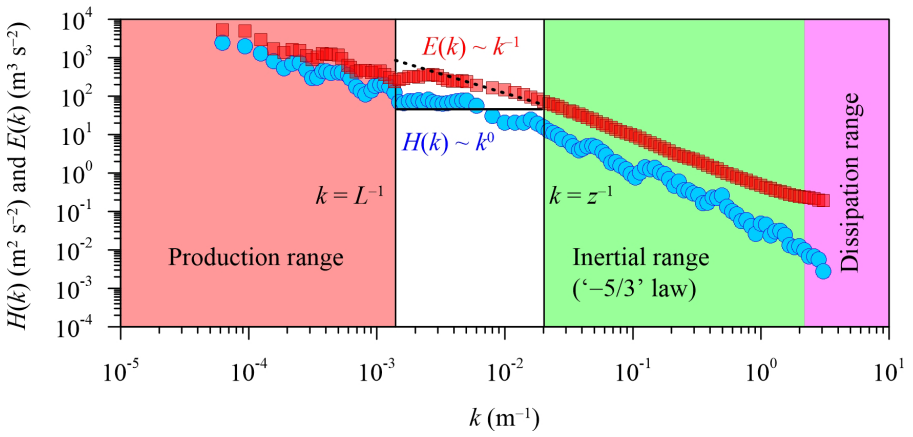

FIG. 3. Helicity spectrum $H(k)$ (circles) and energy spectrum $E(k)$ (squares) obtained from measurements.[4] The spectral behaviors in different ranges include the following: (i) the production range ($k \le L^{-1}$); (ii) the pre-inertial range ($L^{-1} < k \le z^{-1}$), where $\varepsilon(k)$ and $\eta(k)$ obey $\varepsilon(k) \sim k$ and $\eta(k) \sim k^2$, respectively; (iii) the inertial range ($z^{-1} < k < k_d$), where $\varepsilon(k)$ and $\eta(k)$ are independent of k as $\varepsilon(k) = \varepsilon_I$ and $\eta(k) = \eta_i$; and (iv) the dissipation range ($k \ge k_d$). The pre-inertial range evidences the zeroth law of helicity spectrum (solid line, given by $H(k) \sim k^0$). The '−1' spectral law of energy spectrum (broken line, given by $E(k) \sim k^{-1}$) is also preserved in the pre-inertial range.

the experimental data of $H(k)$ support the zeroth law [$H(k) \sim k^0$] quite well in the entire pre-inertial range. For the $H(k)$, the total number of data points in the pre-inertial range ($L^{-1} < k \le z^{-1}$ i.e., 1.4×10^{-3} m^{-1} $< k \le 2.2 \times 10^{-2}$ m^{-1}) is 23.

In this context, one may raise a question whether the experimentally observed helicity spectrum supporting the zeroth law is accidental or genuine. It is worth mentioning that the experimental data of helicity spectrum were not fitted by the relationship $H(k) \sim k^0$ to establish the zeroth law. Moreover, there has not been any direct speculation about the trend of the helicity spectrum to seek the zeroth law. In fact, there remains a concrete conceptual framework underlying the zeroth law of helicity spectrum. Therefore, agreement between the theoretically anticipated zeroth law and the experimentally observed spectrum is not accidental. To substantiate this argument further, the experimentally observed energy spectrum $E(k)$ is shown in Fig. 3. In the pre-inertial range, the experimental data of the energy spectrum convincingly evidence the '−1' spectral law [$E(k) \sim k^{-1}$], as discussed previously.

With regard to the helicity spectrum, it remains an open question as to how the zeroth scaling range evolves when the control parameters (i.e., the Reynolds number or the sensor position) are changed. High-fidelity experimental and numerical data would help to get a satisfactory answer to this question. Moreover, experimental data having different boundary conditions and longer sampling durations are required in order to substantiate the accuracy of the zeroth law.

In essence, the present phenomenological model perfectly predicts the zeroth law in the pre-inertial range. In this context, we remark that the proposed phenomenological model applies for large Reynolds numbers, which establish a prolonged inertial range, so that the presence of dynamic phase orientation between velocity and vorticity fluctuations supports the forward joint cascade of energy and helicity.[3]

IV. CONCLUSION

We discover the zeroth law of helicity spectrum in the pre-inertial range of wall turbulence explaining its origin by the superposition effect of forward joint cascade of energy and helicity transmitted from wall-attached superstructures subject to twisting and stretching. The newly coined zeroth law is preserved in the wavenumber range $L^{-1} < k \le z^{-1}$, which matches satisfactorily with the experimental data.

ACKNOWLEDGMENTS

S.Z.A. acknowledges the Institute Seed Grant of IIT Hyderabad in carrying out this research. S.D. acknowledges the J C Bose Fellowship Award (Funded by DST | Science and Engineering Research Board (SERB), Grant Reference No. JCB/2018/000004) in pursuing this work. We thank O. Chkhetiani for providing the experimental data of helicity spectrum.

AUTHOR DECLARATIONS

Conflict of Interest

The authors have no conflicts to disclose.

Author Contributions

Sk Zeeshan Ali: Conceptualization (equal); data curation (equal); formal analysis (equal); Funding acquisition (equal); investigation (equal); methodology (equal); resources (equal); validation (equal); visualization (equal); Writing – original draft (lead); Writing – review and editing (equal). **Subhasish Dey:** Conceptualization (equal); data curation (equal); formal analysis (equal); funding acquisition (equal); investigation (equal); methodology (equal); resources (equal); validation (equal); visualization (equal); supervision (lead); project administration (lead); Writing – original draft (supporting); writing – review and editing (equal).

DATA AVAILABILITY

The data that support the findings of this study are available from the corresponding authors upon reasonable request.

REFERENCES

[1] H. K. Moffatt, "The degree of knottedness of tangled vortex lines," J. Fluid Mech. **35**(1), 117–129 (1969).

[2] A. Brissaud, U. Frisch, J. Leorat, M. Lesieur, and A. Mazure, "Helicity cascades in fully developed isotropic turbulence," Phys. Fluids **16**(8), 1366–1967 (1973).

[3] L. M. Milanese, N. F. Loureiro, and S. Boldyrev, "Dynamic phase alignment in Navier-Stokes turbulence," Phys. Rev. Lett. **127**(27), 274501 (2021).

[4] B. M. Koprov, V. M. Koprov, V. M. Ponomarev, and O. G. Chkhetiani, "Experimental studies of turbulent helicity and its spectrum in the atmospheric boundary layer," Dokl. Phys. **50**, 419–422 (2005).

[5]V. Borue and S. A. Orszag, "Spectra in helical three-dimensional homogeneous isotropic turbulence," Phys. Rev. E **55**(6), 7005–7009 (1997).
[6]Q. Chen, S. Chen, and G. L. Eyink, "The joint cascade of energy and helicity in three-dimensional turbulence," Phys. Fluids **15**(2), 361–374 (2003).
[7]Q. Chen, S. Chen, G. L. Eyink, and D. D. Holm, "Intermittency in the joint cascade of energy and helicity," Phys. Rev. Lett. **90**(21), 214503 (2003).
[8]G. Sahoo, M. D. Pietro, and L. Biferale, "Helicity statistics in homogeneous and isotropic turbulence and turbulence models," Phys. Rev. Fluids **2**(2), 024601 (2017).
[9]E. Deusebio and E. Lindborg, "Helicity in the Ekman boundary layer," J. Fluid Mech. **755**, 654–671 (2014).
[10]S. Kurien, M. A. Taylor, and T. Matsumoto, "Cascade time scales for energy and helicity in homogeneous isotropic turbulence," Phys. Rev. E **69**(6), 066313 (2004).
[11]G. L. Eyink, "Multi-scale gradient expansion of the turbulent stress tensor," J. Fluid Mech. **549**, 159–190 (2006).
[12]Z. Yan, X. Li, and C. Yu, "Scale locality of helicity cascade in physical space," Phys. Fluids **32**(6), 061705 (2020).
[13]Z. Yan, X. Li, C. Yu, J. Wang, and S. Chen, "Dual channels of helicity cascade in turbulent flows," J. Fluid Mech. **894**, R2 (2020).
[14]I. Marusic, R. Mathis, and N. Hutchins, "Predictive model for wall-bounded turbulent flow," Science **329**(5988), 193–196 (2010).
[15]N. Hutchins, K. Chauhan, I. Marusic, J. Monty, and J. Klewicki, "Towards reconciling the large-scale structure of turbulent boundary layers in the atmosphere and laboratory," Boundary-Layer Meteorol. **145**(2), 273–306 (2012).
[16]H. Qi, X. Li, and C. Yu, "Subgrid-scale helicity equation model for large-eddy simulation of turbulent flows," Phys. Fluids **33**(3), 035128 (2021).
[17]A. A. Townsend, *The Structure of Turbulent Shear Flow* (Cambridge University Press, Cambridge, 1976).
[18]S. Z. Ali and S. Dey, "The law of the wall: A new perspective," Phys. Fluids **32**(12), 121401 (2020).
[19]V. Nikora, "Origin of the '−1' spectral law in wall-bounded turbulence," Phys. Rev. Lett. **83**(4), 734–736 (1999).